Science of the Total Environment 866 (2023) 161375

Contents lists available at ScienceDirect

Science of the Total Environment

journal homepage: www.elsevier.com/locate/scitotenv

Higher toxicity induced by co-exposure of polystyrene microplastics and chloramphenicol to *Microcystis aeruginosa*: Experimental study and molecular dynamics simulation

Na Li [a,b], Zhuotong Zeng [c], Yafei Zhang [a,b], Hui Zhang [a,b], Ning Tang [a,b], Yihui Guo [a,b], Lan Lu [a,b], Xin Li [a,b], Ziqian Zhu [a,b], Xiang Gao [a,b], Jie Liang [a,b,*]

[a] College of Environmental Science and Engineering, Hunan University, Changsha 410082, PR China
[b] Key Laboratory of Environment Biology and Pollution Control, Hunan University, Ministry of Education, Changsha 410082, PR China
[c] Department of Dermatology, Second Xiangya Hospital, Central South University, Changsha 410011, Hunan, PR China

HIGHLIGHTS

- The co-exposure of mPS and CAP induced higher toxicity than the single exposure.
- CAP aggravated the photosynthetic inhibition in the joint group.
- The presence of mPS increased oxidative stress and cell membrane damage.
- CAP altered the conformations of proteins and competed for functional sites.

GRAPHICAL ABSTRACT

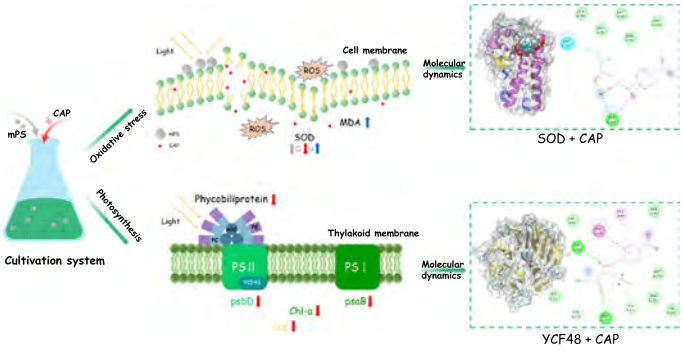

ARTICLE INFO

Editor: Damià Barceló

Keywords:
Micro-polystyrene
CAP
Combined toxicity
Molecular modeling
Proteins

ABSTRACT

Antibiotics and microplastics (MPs) inevitably coexist in natural waters, but their combined effect on aquatic organisms is still ambiguous. This study investigated the individual and combined toxicity of chloramphenicol (CAP) and micro-polystyrene (mPS) particles to *Microcystis aeruginosa* by physiological biomarkers, related gene expression, and molecular dynamics simulation. The results indicated that both individual and joint treatments threatened algal growth, while combined toxicity was higher than the former. Photosynthetic pigments and gene expression were inhibited by single CAP and mPS exposure, but CAP dominated and aggravated photosynthetic toxicity in combined exposure. Additionally, mPS damaged cell membranes and induced oxidative stress, which might further facilitate the entry of CAP into cells during co-exposure. The synergistic effect of CAP and mPS might be explained by the common photosynthetic toxicity target of CAP and mPS as well as oxidative stress. Furthermore, the molecular dynamics simulation revealed that CAP altered conformations of photosynthetic assembly protein YCF48 and SOD enzyme, and competed for functional sites of SOD, thus disturbing photosynthesis and antioxidant systems. These findings provide useful insights into the combined toxicity mechanism of antibiotics and MPs as well as highlight the importance of co-pollutant toxicity in the aquatic environment.

1. Introduction

Antibiotics play an important role in human health and animal husbandry. Antibiotics or their active metabolites can be excreted in urine and feces (Song et al., 2018; Zhou et al., 2021b) and enter the aquatic

* Corresponding author at: College of Environmental Science and Engineering, Hunan University, Changsha 410082, PR China.
E-mail address: liangjie@hnu.edu.cn (J. Liang).

http://dx.doi.org/10.1016/j.scitotenv.2022.161375
Received 2 November 2022; Received in revised form 23 December 2022; Accepted 31 December 2022
Available online 6 January 2023

environment with hospital wastewater, sewage treatment plants, and agricultural runoff (Luo et al., 2019). Antibiotics were frequently detected at concentrations of ng/L to μg/L in the aquatic environment (Li et al., 2018b; Wang et al., 2021). The continuous input into the aquatic ecosystem poses a potential threat to organisms, which has aroused great attention (Gopal et al., 2021; Wang et al., 2020b; Yan et al., 2015). A similar situation also exists for microplastics (MPs). MPs have been found in waters all over the world (Li et al., 2018a; Trevisan et al., 2019). The environmental concentration of MPs in Taihu Lake was found to range from 30 mg/L to 50 mg/L (Mao et al., 2018; Su et al., 2016). Their adverse effects on aquatic organisms (such as plankton (Botterell et al., 2020; Zheng et al., 2022), benthos (Zhang et al., 2021), and vertebrates (Huang et al., 2022)) have also drawn increasing concerns in recent years (Zhang et al., 2022d). Due to overuse and mismanagement, antibiotics and MPs can impact aquatic organisms and even human health through food chains and direct exposure (Zhang et al., 2022a; Zhou et al., 2021b).

Microalgae act as primary producers in the aquatic ecosystem (Zhou et al., 2021a). There have been many studies on the single toxicity of antibiotics or MPs to them. Erythromycin (10–40 μg/L) have been shown to inhibit the growth and photosynthesis of *Microcystis flos-aquae* after 7-d exposure (Wan et al., 2015). Besides, the protein synthesis of *Synechocystis* sp. PCC6803 was also vastly decreased by chloramphenicol (2 mg/L) after a 96 h toxicity test (You et al., 2021). In addition, chlorophyll *a* and photosynthetic activity parameters of *Microcystis flos-aquae* were also reduced by MPs (50–500 mg/L polypropylene and polyvinyl chloride microplastics) after 7-d exposure (Wu et al., 2019). Nylon microplastics (25, 50, 100 mg/L) could induce oxidative stress and disrupt energy metabolism in *Microcystis aeruginosa* after 30-d exposure (Zheng et al., 2022). Nevertheless, the joint toxicity of antibiotics and MPs to algae remains controversial, which needs to be more explicit as they inevitably coexist in natural waters. Antibiotics can be adsorbed on the surface of MPs, which may exhibit different joint toxicity (Wang et al., 2021). Antibiotics (sulfamethoxazole and ibuprofen) presented an antagonistic effect with polystyrene MPs because the adsorption reduced the bioavailability (Li et al., 2022; Wang et al., 2020a). Conversely, Feng et al. argued that the adsorbed tetracycline on polystyrene MPs reduced the electrostatic barrier between polystyrene and *Skeletonema costatum*, resulting in stronger cell-particle interactions and toxicity (Feng et al., 2020). And when polystyrene MPs interacted with algal cells, the adsorbed tetrabromobispheol A was released into cells, increasing joint toxicity (Zhang et al., 2022b). Moreover, the same biological target (cell walls) of doxycycline and MPs (red fluorescent polymer microspheres) might also enhance toxicity of marine microalga *Tetraselmis chuii* (Prata et al., 2018). Hence, joint toxicity is related to their mutual interactions, the altered physicochemical properties, the uptake of antibiotics, and the same biological targets. Considering the complex and inexplicable combined toxicity between antibiotics and MPs, it is vital to explore their joint toxic mechanisms.

As we all know, the presented toxicity is actually regulated by DNA, RNA, and proteins at the molecular level. Proteins are involved in nearly all cellular activities (Liu et al., 2016). Antibiotics severely disturbed photosynthesis-related protein expressions according to proteomic analysis, such as the PSII proteins (psbA, psbD, and psbF), PSI proteins (psaA and psaB), carbon fixation protein (cbbL), and electron transfer proteins (petE and petF) (Jiang et al., 2021; You et al., 2021). MPs cannot directly enter cells but can interact with the cell membrane, inducing a cellular antioxidant response (Liu et al., 2020; Zheng et al., 2022). The current physiological biomarkers and proteomics are insufficient to reveal the interactions between antibiotics and photosynthesis-related proteins. However, with the rapid development of bioinformatics, molecular modeling (molecular docking and dynamics simulation) has emerged as an important tool to disclose the interactions between pollutants and proteins (Lin et al., 2021; Wang et al., 2022). For example, the molecular dynamics (MD) simulation method revealed that pollutants competed with CO_2 for binding to the active sites in the protein Rubisco (Zhang et al., 2022c). Therefore, the introduction of molecular modeling is conducive to revealing toxicity mechanisms at the molecular level.

Microcystis aeruginosa (*M. aeruginosa*), the dominant species causing cyanobacterial blooms, is one of the most widespread primary producers in freshwater ecosystems (Ye et al., 2022). Moreover, *M. aeruginosa*, as a prokaryote, is commonly used as a classic biological model for the research of aquatic pollution and ecotoxicology (Hu et al., 2022) because it is more sensitive to antibiotics than eukaryotic microalgae (Valitalo et al., 2017). Chloramphenicol (CAP) is the antibiotic frequently detected (Jin et al., 2019a). The concentration of CAP in municipal sewage was up to 47 μg/L in Guiyang City, China (Liu et al., 2009). In this study, CAP and the commonly used micro-polystyrene (mPS) (Kik et al., 2020) were selected as target pollutants. We hypothesized that combined exposure of CAP and mPS to *M. aeruginosa* might exhibit a synergistic effect due to a common target (photosynthesis) (You et al., 2021; Zheng et al., 2022). We evaluated physiological biomarkers, including growth inhibition, photosynthetic pigments, and antioxidant activity. Furthermore, related gene transcription and molecular modeling were also used to further explore the toxicity mechanism. This study is expected to provide insight into the toxicological research of MPs and antibiotics in the aquatic environment.

2. Materials and methods

2.1. Chemicals and materials

The suspension of micro-polystyrene (mPS) particles (~1 μm) was purchased from Ruige Biotechnology Co., Ltd. (Jiangsu, China) with an initial concentration of 2.5 % (*w/v*) (reference code: PS01U001NA). The dispersant for mPS was deionized water, according to the manufacturer's information. Dynamic Light Scattering (DLS) (Zetasizer Nano ZS, Malvern, UK) was used to measure the zeta potential and hydrodynamic diameter of mPS in deionized water and BG-11 medium at different experimental concentrations (10, 20, 50 mg/L mPS) (Table S1). Meanwhile, the data on hydrodynamic diameter were used to obtain histograms of the diameter distribution (Fig. S1). Besides, the composition of mPS was determined via Nicolet iN 10™ micro-FTIR (Thermo Electron Scientific Instruments, Madison, WI, USA) (Fig. S2). CAP (98 %) was obtained from MACKLIN reagent Co., Ltd. (Shanghai, China). BG-11 medium was bought from Qingdao Hope Bio-Technology Co., Ltd. Analytical grade reagents were used in the experiment. CAP solution (250 mg/L) and mPS suspension (500 mg/L) were prepared before experiments.

2.2. M. aeruginosa cultivation and exposure experiment

The freshwater algae *M. aeruginosa* FACHB-912 (single cells) was obtained from the Institute of Hydrobiology, Chinese Academy of Sciences (Wuhan, China). The detailed cultivation of *M. aeruginosa* was shown in Supporting Information, Text S1. After the algal cells were cultured and activated three times, the algal cells in the logarithmic growth phase were taken for 96 h toxicity tests. According to previous studies (You et al., 2021; Zhang et al., 2022d) and the preliminary experiments, CAP concentrations of 0.5, 1.0, 1.5, 2.0, 5.0, and 10 mg/L were selected in the single toxicity tests to calculate the EC50 value. And the concentration of CAP was fixed at 3 mg/L in the co-exposure groups because it was close to the EC50 value. The mPS concentrations were set to 10, 20, and 50 mg/L based on the environmental abundance (ranging from 30 to 50 mg/L) (Mao et al., 2018; Su et al., 2016). Before the toxicity tests, a stock mPS suspension was ultrasonically dispersed for 30 min. The designated volumes of mPS suspension were immediately added to the BG-11 medium in 250 mL flasks, and the solutions were sonicated again for 15 min to achieve dispersion. Appropriate volumes of CAP solution (250 mg/L) were added to the BG-11 medium. These solutions containing CAP and/or mPS were inoculated with algae. Algal cells without any pollutants were used as the control group. In order to reduce the interference of absorbance, we referred to the experiments of Zhou et al. (Zhou et al., 2021a). The background absorbances of different mPS concentrations in the BG-11 medium without *M. aeruginosa* inoculation were measured before toxicity tests. Background absorbances of mPS were subtracted when calculating cell density. The

growth inhibition rate (IR) was obtained as $IR = 1 - N_c/N_t$, where N_c and N_t are the cell density in the control and treatment groups, respectively. In addition, photosynthetic pigments (chlorophyll *a*, carotenoid, and phycobiliprotein), SOD, and MDA biomarkers were also measured during the experiments. The EC50 of CAP for *M. aeruginosa* was calculated by the dose-response curve, and the joint toxicity was assessed by the independent action (IA) model (Text S2). Moreover, CAP concentration analysis was displayed in Supporting Information, Text S3.

2.3. Analysis of the photosynthetic pigments

The photosynthetic pigment contents were measured after 48 and 96 h exposure. Chlorophyll *a* and carotenoid were determined by 95 % ethanol extraction (Zeng et al., 2021; Zheng et al., 2022). 8 mL of algal cells were taken and centrifuged (H-1850, Xiangyi centrifuge instrument Co., Ltd., Hunan, China) (5000 rpm at 4 °C for 15 min). Then, 5 mL of precooled 95 % ethanol was added for extraction in the dark for 24 h. The mixture was centrifuged at 5000 rpm for 15 min. Subsequently, the supernatant was measured at 470, 649, and 665 nm by a UV-VIS spectrophotometer. Chlorophyll *a* and carotenoid content were calculated by the following equations:

$$\text{Chl}-a\ (\mu g/mL) = (13.7A_{665} - 5.76A_{649}) \times \frac{V_1}{V_2} \quad (1)$$

$$\text{Carotenoid}\ (\mu g/mL) = (1000A_{470} - 2.05C_{\text{Chl a}})/245 \quad (2)$$

where V_1 and V_2 represent 95 % ethanol and sample volume, respectively.

Phycobiliprotein in cyanobacteria mainly includes phycocyanin (PC), allophycocyanin (APC), and phycoerythrin (PE). Phycobiliprotein can harvest wavelengths that chlorophyll *a* and carotenoid cannot absorb (Xu et al., 2021). 8 mL of algal cells were collected and centrifuged. After discarding the supernatant, 8 mL of liquid with precooled buffered saline (0.01 M sodium phosphate, pH = 7.0, and 0.15 M NaCl) was added. Then, the freeze-thaw was repeated three times (freezing temperature: −20 °C, thawing temperature: 20 °C). The mixture was lysed using an ultrasonic cell disruptor (KM-450D, Kunshan Meimei Ultrasonic Instrument Co., Ltd., China) for 5 min (run time: 3 s, rest time: 8 s, 200 W). The broken cell suspensions were centrifuged at 8000 rpm, 4 °C for 15 min. The supernatant was collected to determine the absorbance at 562, 615, and 652 nm by a UV-VIS spectrophotometer. The values of PC, APC, PE, and phycobiliprotein were obtained by the following equations (Bennett and Bogorad, 1973; Bi et al., 2011; Xu et al., 2021):

$$\text{PC}\ (mg/mL) = (A_{615} - 0.474A_{652})/5.34 \quad (3)$$

$$\text{APC}\ (mg/mL) = (A_{652} - 0.208A_{615})/5.09 \quad (4)$$

$$\text{PE}\ (mg/mL) = (A_{562} - 2.41C_{\text{PC}} - 0.849C_{\text{APC}})/9.62 \quad (5)$$

$$\text{Phycobiliprotein}\ (mg/mL) = \text{PC} + \text{APC} + \text{PE} \quad (6)$$

2.4. Analysis of the antioxidant enzyme

After 96 h toxicity tests, 20 mL of algal cells were centrifuged (5000 rpm at 4 °C for 15 min). The algal cell was washed twice with phosphate-buffered saline (0.05 M, pH = 7.8), and then 2 mL of precooled phosphate-buffered saline was added. The mixture was lysed by an ultrasonic cell disruptor for 5 min and then centrifuged at 5000 rpm, 4 °C for 15 min to obtain the supernatant. The superoxide dismutase (SOD) and malondialdehyde (MDA) contents were measured using the assay kits (A001–1, A003–1, Nanjing Jiancheng Bioengineering Institute, China). The supernatant was measured at 550 and 532 nm using a UV-VIS spectrophotometer to calculate the SOD and MDA contents, respectively.

2.5. Morphologic properties and real-time quantitative PCR

After 96 h toxicity tests, the algal cells of four groups (control, 3 mg/L CAP, 50 mg/L mPS, 3 mg/L CAP +50 mg/L mPS) were centrifuged (5000 rpm at 4 °C for 15 min). The pellets were fixed with precooled 2.5 % glutaraldehyde. The cells were washed twice with phosphate buffer (0.1 M, pH = 7), and then dehydrated by ethanol solutions with gradient concentrations (30 %, 50 %, 70 %, 80 %, 90 %, 95 %, and 100 %). The ethanol solution of each gradient was added to algal cells for 10 min, and then the cells were collected by centrifugation. The samples were freeze-dried before observation in the scanning electron microscope (FEI Nova Nano 450, Hillsboro, USA).

The algal cells were collected after 96 h toxicity tests by centrifugation (4000 rpm at 4 °C for 15 min). The cells were quickly frozen with liquid nitrogen and stored at −80 °C until RNA extraction. 1.5 % agarose RNA electrophoresis and A_{260nm}/A_{280nm} values were used to detect the RNA quality. Total RNA was reversely transcribed into cDNA using a Maxima Reverse Transcriptase kit. And Quantitative real-time PCR was measured by QuantStudio 3&5 Real-time PCR detection System (Thermo Fisher, USA) and the SybrGreen qPCR Master Mix kit (Applied Biosystems, USA). The 16S rRNA was selected as an internal reference gene. Three target genes (*psaB*, *psbD*, and *sod*) were determined in this study because these genes are related to photosynthesis and antioxidant systems. All primer sequences and functions of genes were displayed in Supporting Information, **Table S2**.

2.6. Molecular docking and MD simulation

The detailed processes of molecular docking and MD simulation were described in **Text S4**. Briefly, the protein sequences were obtained from the NCBI protein database (https://www.ncbi.nlm.nih.gov/protein/). And the structures of YCF48 and SOD of *M. aeruginosa* were obtained by homology modeling. The results of nomology modeling were verified whether the structures were reasonable. The CAP structure was downloaded from the NCBI PubChem database. Then, the molecular docking of proteins and CAP was performed using Autodock vina 1.1.2. The best conformation with a reasonable structure was used to perform the MD simulation by GROMACS 2020.4 software. The MD simulation was mainly carried out through system initialization, energy minimization, preequilibrium (NVT and NPT), production molecular simulation, and analysis procedures. Root mean square deviation (RMSD) and radius of gyration (Rg) were used to check whether the system was stable. The simulated trajectories were analysed. Moreover, the results were visualized using VMD, PyMOL 2.5.0, and Biovia Discovery Studio Visualizer software. The binding free energy was calculated using the molecular mechanics Poisson-Boltzmann surface area (MM-PBSA) method.

2.7. Statistical analysis

All toxicity experiments were conducted in three replicates. Parametric data were presented by mean ± standard deviation. Non-parametric data were expressed by median and interquartile. Statistical analysis was determined using one-way ANOVA, the non-parametric Kruskal-Wallis test, two-way ANOVA, and repeated measure ANOVA. The Tukey HSD test (parametric data) and Dunn's test (nonparametric data) were used for the multiple comparisons. The significant difference was defined as $p < 0.05$, and $p < 0.01$ was considered an extremely significant difference. The data analysis and visualization were conducted using the following software: IBM SPSS 21.0 and OriginPro 2022b.

3. Results and discussion

3.1. Growth inhibition of M. aeruginosa induced by CAP and mPS

The cell density of CAP-exposed groups was significantly reduced compared with the control group **(Fig. S3a)** ($df = 6$, $F = 300.62$, $p < 0.001$). A

significant negative correlation was found between CAP concentration and cell density (**Table S3, 4**), consistent with the observed trend. Thus, the concentration-dependent inhibitory effect was shown in CAP groups. The dose-response curve **(Fig. S4a)** indicated that the 96 h EC50 value was 3.70 mg/L. Similar to this value, the EC50 values of CAP for *Synechocystis* sp. PCC6803, *Pseudokirchneriella subcapitata*, and *Scenedesmus acuminatus* were 3.76, 2.71, and 2.28 mg/L, respectively (Xiong et al., 2019; You et al., 2021). Moreover, CAP concentration and growth inhibition had a positive correlation (**Table S3**), and the EC50 value (4.38 mg/L) obtained from the probit regression analysis (**Table S5**) was close to the calculated value (3.70 mg/L) by fitting the dose-response curve. In the individual mPS exposure **(Fig. S3b)**, the growth inhibition rates for 10, 20, and 50 mg/L mPS reached 10.86 %, 12.08 %, and 45.87 %, respectively. These results indicated the toxicity increased with increasing concentrations of mPS.

The algal growth showed significant inhibition ($p < 0.01$) in all treatment groups compared with the control group after 96 h exposure **(Fig. S3b)**. The results of the repeated measure ANOVA also implied that cell density of *M. aeruginosa* was significantly influenced by time, treatment, and their interaction (**Table S6**). After 96 h exposure, the order of growth inhibition was 10 mg/L mPS < 20 mg/L mPS < CAP < CAP +10 mg/L mPS < 50 mg/L mPS < CAP +20 mg/L mPS < CAP +50 mg/L mPS, indicating that co-exposure induced a higher growth inhibition than individuals. Correspondingly, the result of the independent action (IA) model also exhibited a synergistic effect between CAP and mPS on *M. aeruginosa* **(Table S7)**. The combined toxicity to algae is frequently determined by the interactions of co-pollutants. The interactions can present antagonistic toxicity by decreasing bioavailability, while no interactions may show higher toxicity (You et al., 2021; You et al., 2022; Zhang et al., 2022d). The two-way ANOVA analysis (**Table S8**) indicated that CAP concentration was only affected by time due to the biodegradation of antibiotics by algal cells over time (Xiong et al., 2021), but no obvious differences in CAP concentration were found among all treatments at same exposure time **(Fig. S4b, Table S8)**. Hence, there seemed to be no significant interaction between mPS and CAP, which explained the synergistic effect. The above results revealed that the toxicity of mixed exposure was stronger than that of the individual group.

3.2. Effects of CAP and mPS on photosynthetic pigments and genes (psaB and psbD) of M. aeruginosa

Photosynthesis is an essential mode of energy metabolism in microalgae. The photosynthetic pigments can largely reflect the photosynthetic capacity (Simkin et al., 2022). Thus, the photosynthetic pigments (chlorophyll *a*, carotenoid, phycobiliprotein) were measured to indicate the impact on the growth of *M. aeruginosa*. Incubation time, different treatments, and their interaction all had obvious influences on the photosynthetic pigments of *M. aeruginosa* (**Table S9**). Therefore, the responses of pigments to the single and joint exposure at different times were discussed. In the 10, 20, and 50 mg/L mPS-exposed groups, the chlorophyll *a* content was reduced by 10.35–21.24 % relative to the control at 48 h **(**Fig. 1a**)** ($df = 7$, $F = 56.13$, $p < 0.001$). After 96 h mPS exposure, chlorophyll *a* was decreased by 7.78–12.40 % compared with the control group **(**Fig. 1b**)** ($df = 7$, $F = 46.89$, $p < 0.001$). The content of carotenoid was decreased by 4.69–13.36 % at 48 h mPS exposure **(**Fig. 1c**)** ($df = 7$, $F = 52.94$, $p < 0.001$) but recovered after 96 h exposure **(**Fig. 1d**)** ($df = 7$, $F = 58.02$, $p < 0.001$). Similarly, the content of phycobiliprotein was downregulated during mPS exposure (Fig. 1e) ($df = 7$, $F = 16.34$, $p < 0.001$), and then gradually recovered **(**Fig. 1f**)** ($df = 7$, $F = 9.45$, $p < 0.001$). Possible explanations for these occurrences were as follows: (1) *M. aeruginosa* upregulated carotenoid and phycobiliprotein content to maintain the stability of cells due to the reduction of chlorophyll *a* (Mao et al., 2020). (2) Carotenoid and phycobiliprotein have the antioxidant effect (Zheng et al., 2022; Zhou et al., 2018), thus increasing the content of both to alleviate peroxidative damage.

In the single CAP exposure group, photosynthetic pigments continued to reduce with time **(**Fig. 1**)**. Previous studies have confirmed that CAP is an inhibitor of photosynthesis (Kodru et al., 2020; Okada et al., 1991). After 48 h exposure, the contents of chlorophyll *a* and carotenoid in the mixed group were lower than those in the CAP or mPS alone **(**Fig. 1a, c**)**. Notably, the photosynthetic pigments content of the co-exposure group was not decreased with the increase of mPS concentration during the experiment, except for phycobiliprotein content at 48 h. The increase in mPS concentration seemed to have no obvious effect on photosynthetic pigments in the mixed group. And no significant difference ($p > 0.05$) was observed in the content of photosynthetic pigments between the mixed group and CAP group at 96 h. These results implied CAP might dominate photosynthetic pigments inhibition in the co-exposed group. The decrease in photosynthetic pigments caused by mPS could be alleviated by cell self-regulation, while the inhibition of protein biosynthesis by CAP (You et al., 2021) would make cells unable to respond to mPS stress. Hence, CAP exposure could aggravate inhibitory effect on photosynthetic pigments in the mixed group.

To further explore photosynthetic toxicity, the expression levels of photosynthesis-related genes *psaB* and *psbD* in *M. aeruginosa* were determined after experiments. As shown in **Fig. S5**, the transcriptional abundances of *psaB* ($df = 3$, $H = 9.80$, $p = 0.02$) and *psbD* ($df = 3$, $H = 10.53$, $p = 0.02$) were obviously inhibited in different treatment groups. In the single mPS exposure, *psaB* and *psbD* expressions decreased to approximately 0.72 and 0.53-fold relative to controls. *M. aeruginosa* can adsorb MPs, and the size (~1 μm) of MPs used for this experiment was larger than the visibility wavelength (390–760 nm) (Liu et al., 2020). Therefore, mPS can obstruct the light and thus inhibit photosynthesis. After exposure to CAP, the abundances of *psaB* and *psbD* were dramatically downregulated to 0.15 and 0.39-fold relative to controls, indicating CAP damaged photosynthesis more severely than mPS. In the co-exposed group, the *psaB* and psbD expressions were significantly lower than that of the control. The photosynthetic genes inhibition and light obstruction were induced by CAP and mPS. These results indicated that photosynthesis seemed to be the common goal of CAP and mPS.

3.3. Oxidative stress of M. aeruginosa induced by CAP and mPS

Reactive oxygen species (ROS) can be produced by algae in an adverse environment, and then antioxidant enzymes, such as superoxide dismutase (SOD), would be increased to clear ROS in the antioxidant system (Li et al., 2022). SOD is the most powerful antioxidant in the cell and is indispensable for cellular health (Ighodaro and Akinloye, 2019), catalyzing the conversion of superoxide radicals into hydrogen peroxide and oxygen (Zheng et al., 2022). MDA, the main biomarker of oxidative stress intensity and lipid peroxidation (Li et al., 2020), was also measured (Li et al., 2022). In the individual mPS exposure, the SOD activity increased from 40 to 62 $U/10^8$ cells with the increase in mPS concentration **(**Fig. 2a**)** ($df = 7$, $F = 14.28$, $p < 0.001$), which was consistent with the concentration-dependent inhibitory effect. The SOD activity in mixed exposures was higher than that of CAP alone, indicating the presence of mPS triggered more SOD production. Furthermore, the transcript levels of *sod* in different treatments were displayed in Fig. 2b ($df = 3$, $F = 172.52$, $p < 0.001$). Interestingly, the abundance of *sod* in the CAP group was significantly downregulated, indicating that CAP might affect SOD synthesis. Similarly, SOD downregulation caused by CAP was also demonstrated through proteomics analysis (You et al., 2021). Compared with the control group or CAP exposure, the expressions of *sod* in mPS and mixed exposures were significantly increased. However, the *sod* abundance of the mixed group was lower than that of single mPS exposure. The result suggested that both CAP and mPS in the co-exposure group had effects on the production of SOD.

In addition, the changes in MDA contents **(**Fig. 2c**)** ($df = 7$, $F = 27.38$, $p < 0.001$) in treatment groups were similar to those of SOD activity. The MDA content in the co-exposure was higher than that in the CAP exposure. The results showed that mPS could induce membrane lipid peroxidation and oxidative stress damage (Zhu et al., 2019) in co-exposures. The

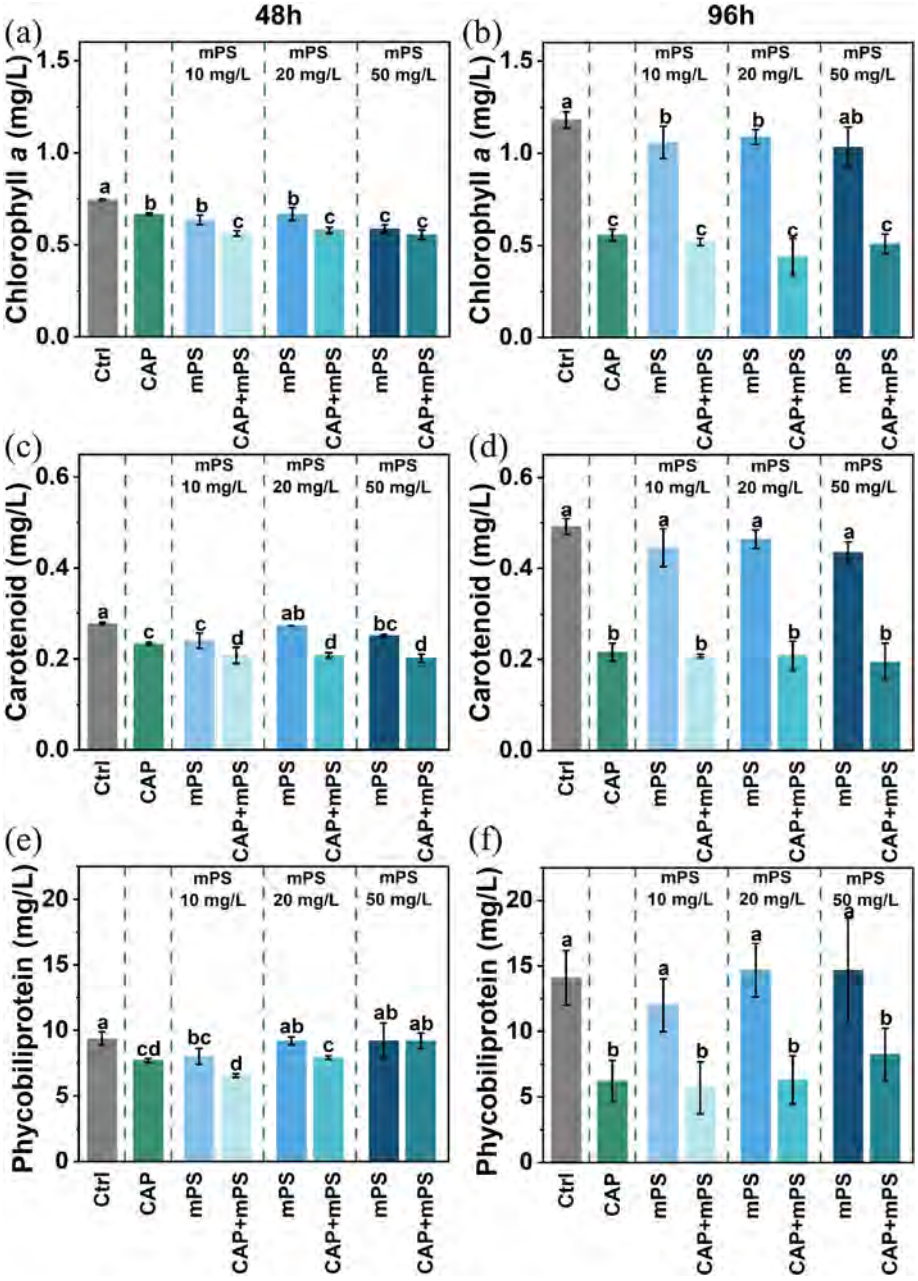

Fig. 1. The content of chlorophyll *a* (a, b), carotenoid (c, d), phycobiliprotein (e, f) for *M. aeruginosa* exposed to chloramphenicol (CAP) or/and micro-polystyrene (mPS) at 48 and 96 h. CAP at a concentration of 3 mg/L and mPS at concentrations of 10, 20, and 50 mg/L. Different letters indicate significant differences among different treatments (one-way ANOVA: $p < 0.05$). Mean ± SD, $n = 3$.

mixed and single mPS exposures significantly increased the MDA content compared to the control group, suggesting that ROS overproduction caused severe lipid peroxidation. Previous studies reported that ROS was not involved in antibiotic toxicity to algae (Keren et al., 2013; You et al., 2022). In this experiment, the reduction of *sod* abundance also supported this result after CAP exposure. Therefore, oxidative stress damage was the primary toxicity of mPS to *M. aeruginosa* in the mixed group. Moreover, the changes in morphologic features were presented through SEM (Fig. 2d). In the CAP exposure group, the wrinkle and final lysis of algal cells might be due to inhibition of cellular biosynthesis and metabolism (You et al., 2021). The adsorption or aggregation between mPS and algae (Fig. 2d) might induce cell membrane physical or oxidative damage, which explained the increase of SOD and MDA contents. And the damage to the membrane might result in the easier entry of CAP into cells (Zhang et al., 2022b), thereby increasing the combined toxicity of CAP and mPS. This finding supported the growth inhibition of *M. aeruginosa*.

3.4. Molecular docking and MD simulation of proteins and CAP

Antibiotics can be absorbed into cells and might further interfere with cellular metabolic activities. Photosynthesis and *sod* abundance were affected by CAP in this experiment. However, it is unknown whether CAP can disturb the function or activity of photosynthesis-related proteins and SOD enzyme by directly changing their conformations. YCF48 protein promotes the formation of assembly intermediate in the PSII reaction center, replaces damaged D1 protein in the process of PSII repair, and can also bind to PSI (Mabbitt et al., 2014; Yu et al., 2018). Hence, the YCF48 protein

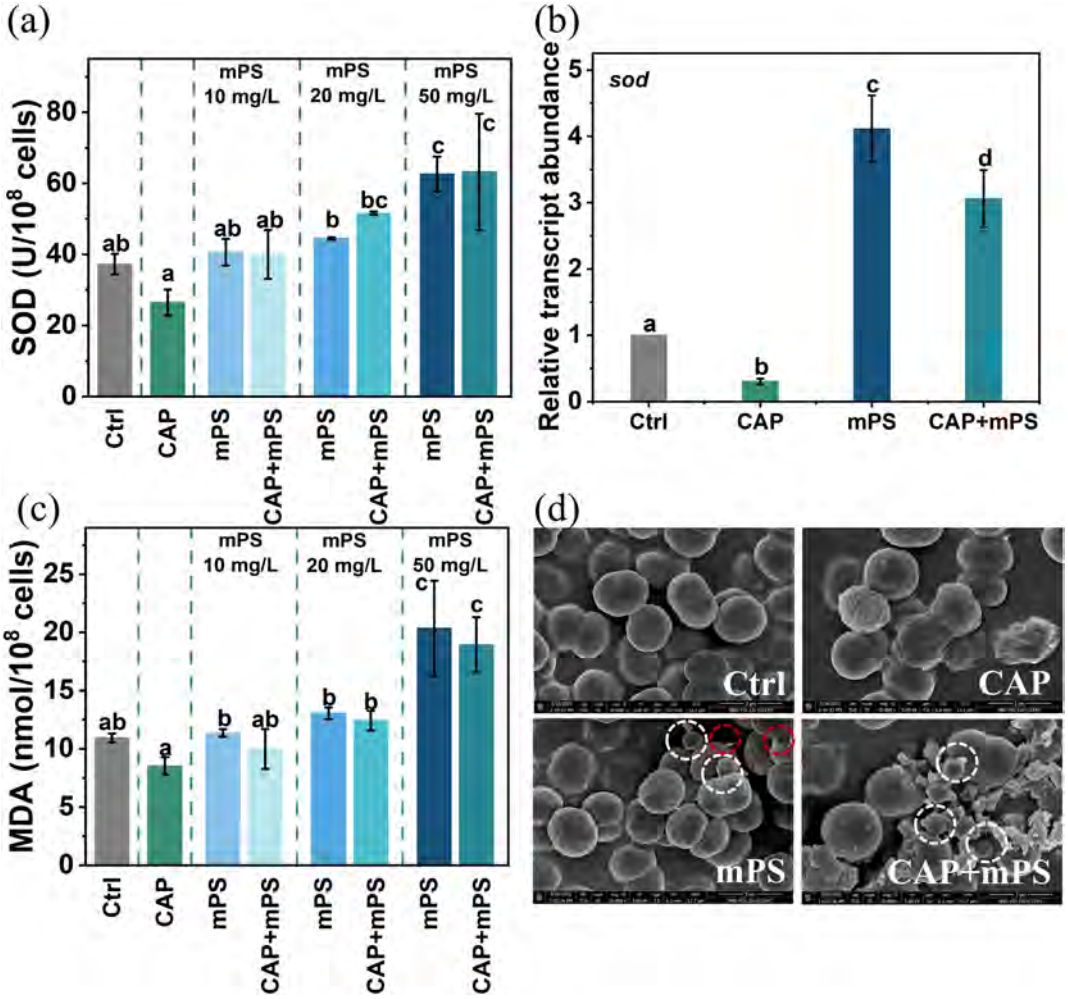

Fig. 2. The contents of SOD (a), MDA (c) for *M. aeruginosa* exposed to chloramphenicol (CAP) and micro-polystyrene (mPS) at 96 h. CAP at a concentration of 3 mg/L and mPS at concentrations of 10, 20, and 50 mg/L. The transcript abundance of *sod* (b) and SEM images (d) for *M. aeruginosa* exposed to CAP (3 mg/L), mPS (50 mg/L), and CAP (3 mg/L) + mPS (50 mg/L) for 96 h (The white dotted circle refers to mPS, and the red represents cell membrane damage). Different letters indicate significant differences among different treatments (one-way ANOVA: $p < 0.05$). Mean ± SD, n = 3.

and SOD enzyme were selected to investigate the binding mechanism between proteins and CAP through molecular docking and MD simulation.

The molecular docking was shown in Fig. 3**.** The minimum binding free energy between YCF48 protein and CAP was −5.90 kcal/mol. CAP formed four stable hydrogen bonds with residues ARG175, TYR130, ARG302, and ASP44, respectively. Moreover, van der Waals, Pi-cation, and alkyl contributed to the binding forces between CAP and YCF48 (Fig. 3a, b**)**. The minimum binding energy of SOD with CAP was −5.60 kcal/mol. CAP presented two hydrogen bonds with SER 161 and GLU200. Pi-Pi T-shaped, alkyl, and Pi-alkyl hydrophobic interactions existed between CAP and three residues (HIS201, LEU205 and PHE58) **(**Fig. 3c, d**)**. Hence, CAP bound well in the active pocket provided by protein YCF48 and SOD.

To explore the dynamic alterations in the binding process of protein-ligand complexes, 50 ns molecular dynamics simulations were performed. The RMSD and Rg are used to judge system equilibrium and to represent the compactness changes of systems (Bhatt et al., 2021), respectively. As shown in Fig. 4a, RMSD values continued to rise during 0–5 ns. RMSD values and the fluctuation were relatively small in the range of 5–50 ns. Therefore, the conformation of protein-ligand complexes was first adjusted in 0–5 ns and then reached equilibrium within 5–50 ns. The RMSD trend of YCF48 protein and YCF48 + CAP complex was consistent, while the RMSD of SOD enzyme was lower than that of SOD + CAP complex. It is commonly considered that the smaller the RMSD value and fluctuation, the more stable the system is (Lin et al., 2021). Therefore, CAP seemed to have no effect on the stability of YCF48 protein, but had a certain inhibitory effect on SOD owing to the difference of RMSD in protein and protein-ligand system (Lin et al., 2021). The Rg values of all systems were generally stable **(**Fig. 4b**)**, which was in accordance with RMSD results. The Rg value of YCF48 was slightly higher than that of YCF48 + CAP complex, whereas the Rg value of SOD groups was the opposite, indicating CAP altered the compactness of both proteins and might further disturb the function of proteins (Li et al., 2021).

To further explore the interaction and conformational changes of the protein-ligand complexes, we analysed the simulated conformational snapshots of MD trajectories at 0, 25, and 50 ns **(**Fig. 5**)**. For the YCF48 + CAP system **(**Fig. 5a, b, c**)**, CAP was bound within the active pocket. At 0 and 25 ns, three hydrogen bonds were formed between CAP and amino acids ASP44, ARG175, and LYS214. But the hydrogen bond with LYS214 disappeared at 50 ns. LYS214 might break away from the active site and lose its effective interaction because of improper rotation. The same phenomenon was also reported that the hydrogen bond disappeared after 75 ns simulation for a similar reason (Hosseini and Amanlou, 2020). van der Waals, electrostatic energy, and hydrophobic interaction were observed between CAP and multiple amino acids, which made CAP remain stable in the active pocket. This result was in accordance with molecular docking and RMSD. For the SOD + CAP system (Fig. 5d, e, f), the residue changes of interactions displayed that CAP in the SOD active pocket had outward movement, which was also seen in Fig. 6a, b, c. At 25 and 50 ns, CAP formed hydrogen

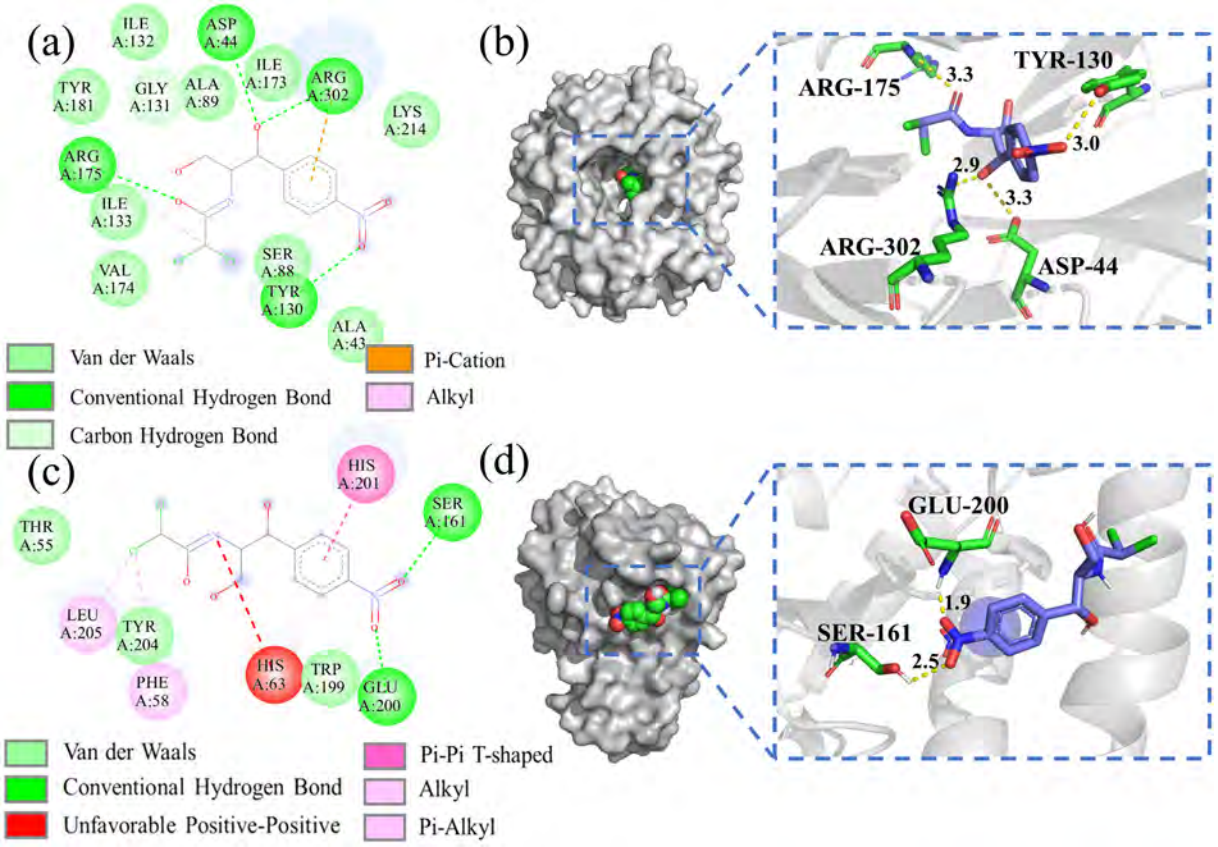

Fig. 3. Molecular docking of chloramphenicol (CAP) with proteins YCF48 (a, b) and SOD (c, d). The two-dimensional interaction diagrams (between amino acids and CAP) on the left, and the three-dimensional active site and hydrogen bond diagrams on the right.

bonds with TYR204 and ARG208, and van der Waals was also observed, preventing CAP from escaping the active pocket. As shown in Fig. 6, the CAP binding site 5 Å region was extracted and superposed to observe structural changes (Chen et al., 2017). For the YCF48 + CAP system, the amino acids in the 5 Å region were similar at 0, 25, and 50 ns, but the conformational changes of amino acids (ILE133, ASP44, and LYS214) were found in the structural superposition (Fig. 6d, e). Moreover, four amino acids (ARG187, ARG206, ARG210, and ARG211) of YCF48 are the binding sites for the photosynthetic D1 protein (Yu et al., 2018). The relative positions and conformations of these four amino acids were observed to change **(Fig. S6)**. For the SOD + CAP system, many conformations of amino acids were also changed in the 5 Å region. Structural changes in amino acids and active pocket movement might lead to protein deformation and function impairment (Chen et al., 2017; Jin et al., 2019b).

The binding free energy (**Table S10**) of CAP and proteins (YCF48 and SOD) was calculated using the MM-PBSA method to better understand the interactions between protein and ligand. The binding free energies of YCF48 + CAP and SOD + CAP were − 34.22 ± 16.91 and − 46.88 ±

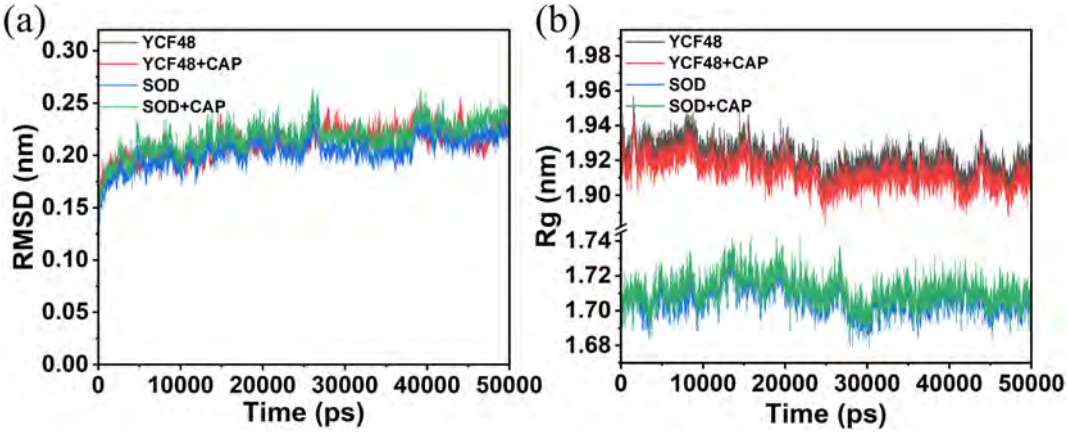

Fig. 4. Root mean square deviation (RMSD) (a) and radius of gyration (Rg) (b) of proteins (YCF48 and SOD) and protein-ligand complexes (YCF48 + CAP and SOD + CAP) during 50 ns simulation. Protein: YCF48 and SOD; CAP: chloramphenicol.

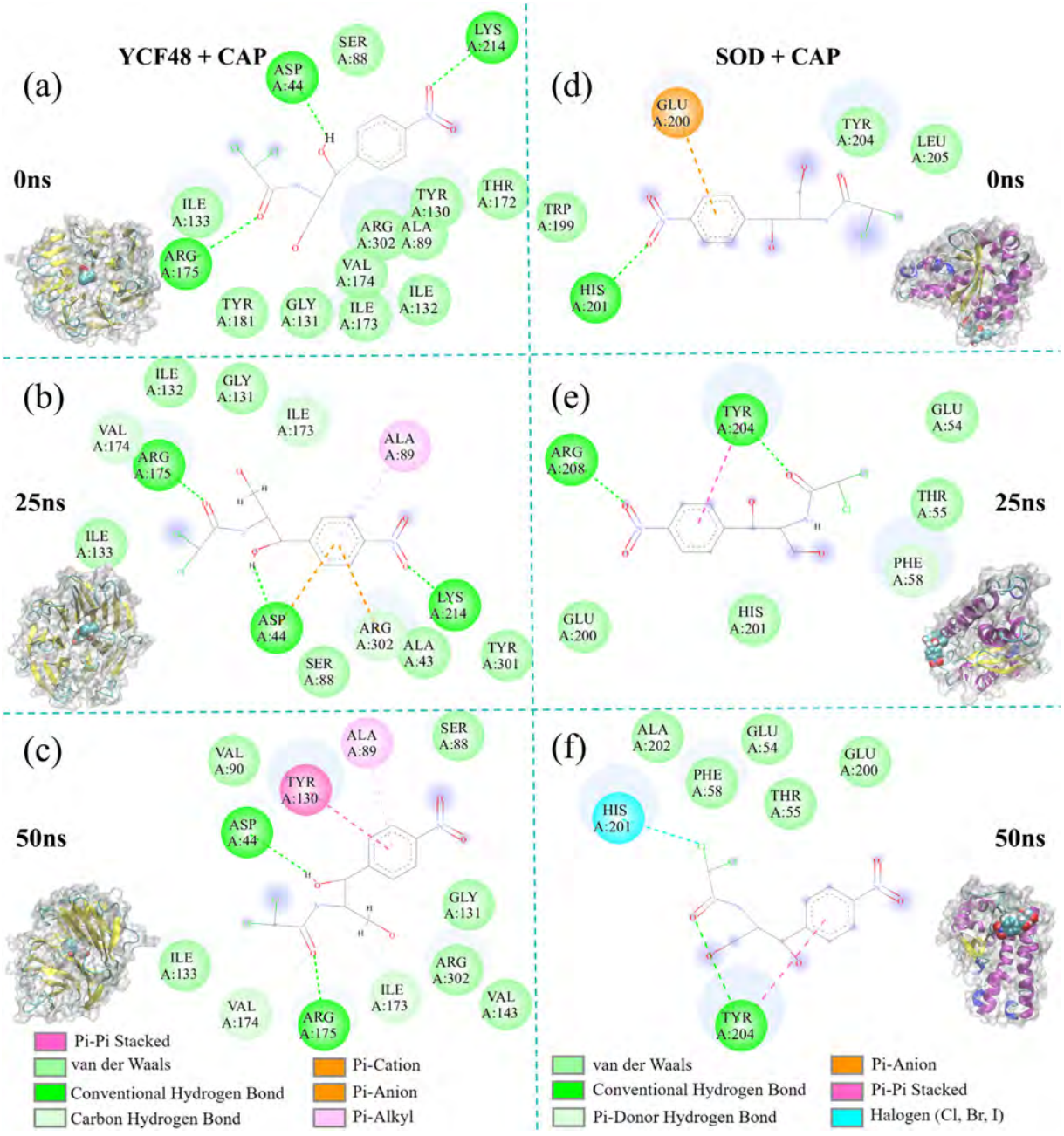

Fig. 5. Three-dimensional conformations and two-dimensional interactions for YCF48 + CAP complex (a-c) and SOD + CAP (e-f) complex after 0, 25, 50 ns simulation. Protein: YCF48 and SOD; CAP: chloramphenicol.

15.82 kJ/mol, displaying that CAP could bind to proteins YCF48 and SOD. However, the binding free energy of YCF48 + CAP was lower than that of SOD + CAP, which was inconsistent with molecular docking and stable binding of YCF48 + CAP complex. The possible reason was that the volume of the binding pocket exposed to solvent was relatively large (Lin et al., 2021), and the polar solvation energy in YCF48 + CAP system was up to 201.78 ± 24.35 kJ/mol, which might weaken the van der Waals and electrostatic energy. According to the calculation and analysis of each energy, the van der Waals was the main driving force for the binding of protein to CAP, and electrostatic energy also contributed greatly to YCF48 + CAP system. Previous studies also demonstrated that van der Waals is the key energy in receptor-ligand molecular simulations (Hosseini and Amanlou, 2020; Li et al., 2021; Liu et al., 2018). The binding free energy of complexes was decomposed into the energy of each amino acid **(Fig. S7)**. For the YCF48 + CAP system **(Fig. S7a)**, amino acids such as VAL174, ALA89, ILE133, and TYR130 played key roles via van der Waals and electrostatic energy (Fig. 5b). But the binding free energies of ASP44, ARG175, and LYS214, which formed hydrogen bonds with CAP, were positive. It was found that the sum of polar solvation and SASA energy was very high **(Fig. S8)**, which weakened the binding energy between amino acids and CAP. For the SOD + CAP system **(Fig. S7b)**, the binding energy of TYR204 to CAP was up to −6.94 kJ/mol. Hydrogen bond and pi-pi stacked interaction were formed between TYR204 and CAP, which was beneficial to the combination. PHE58, GLU54, THR55, and ALA202 also promoted the binding of SOD and CAP by van der Waals. CAP was bound to HIS201 through a halogen bond. And HIS201 is the functional active site and the key amino acid for the symmetric dimer (Atzenhofer et al., 2002). Therefore, the binding process of SOD and CAP might interfere with the functions of SOD.

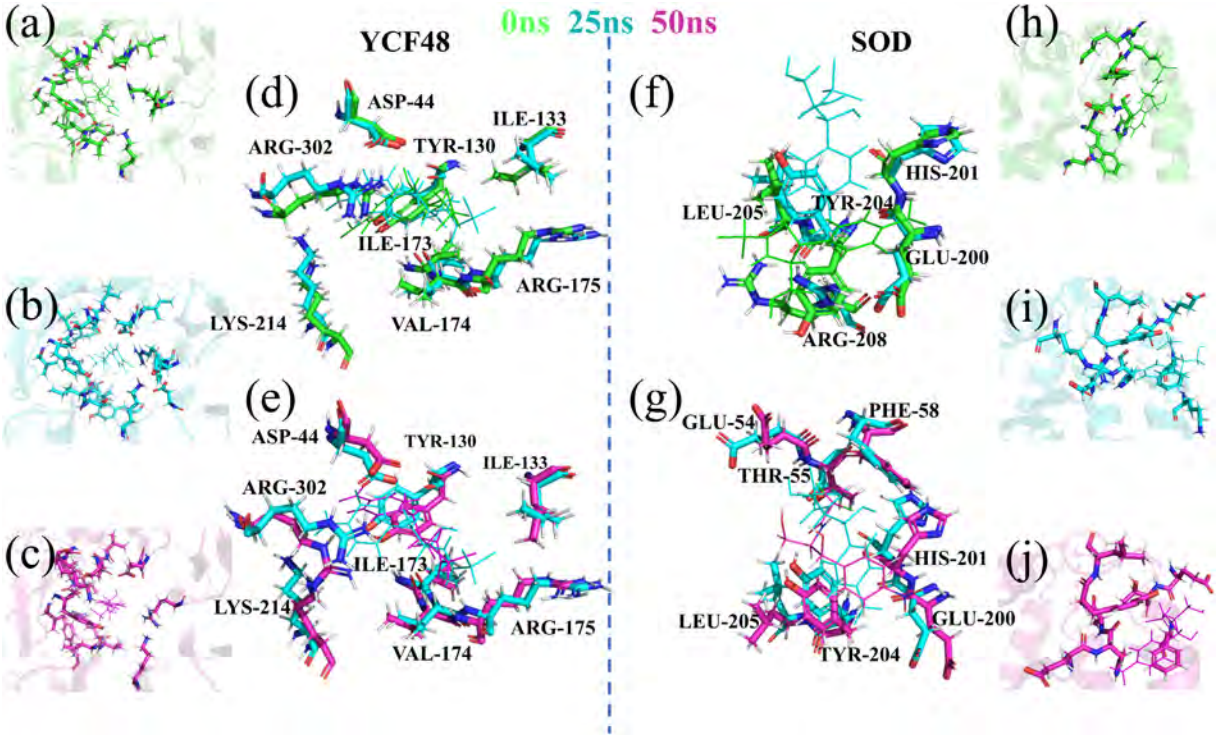

Fig. 6. The chloramphenicol (CAP) binding site 5 Å region with proteins YCF48 (a-c) and SOD (h-j) after 0, 25, 50 ns simulation. And the 0–25 ns and 25–50 ns structures were superimposed on the 5 Å region of proteins YCF48 (d, e) and SOD (f, g) bound to CAP.

In summary, CAP was bound to the active pocket provided by proteins YCF48 and SOD, inducing conformational changes in proteins and competing for functional active sites in SOD enzyme. Thus, photosynthesis and antioxidant systems were affected, which was consistent with experimental results. However, molecular modeling mainly predicts possible interactions of protein-ligand by specific algorithms and scoring functions. It still needs to be validated by some experimental methods.

4. Conclusion

Both antibiotics and microplastics have been widely used in our daily lives. Aquatic organisms are unavoidably exposed to them owing to a series of discharges. Most studies only concentrated on the toxicity of single pollutants to organisms, but the results of mixed toxicity might be more reasonable in the actual environment. In our study, the individual and combined exposures of chloramphenicol and micro-polystyrene to *M. aeruginosa* were explored. Experimental results showed that the toxicity of joint exposure was higher than that of single groups. The levels of photosynthetic pigments and related genes (*psaB* and *psbD*) were inhibited by CAP or mPS. But the photosynthetic pigments were not decreased with the increasing concentration of mPS in mixed exposure, which implied that CAP dominated the photosynthetic inhibition during combined treatment. Oxidative stress might be induced by mPS rather than CAP because mPS exposure significantly upregulated the levels of SOD, MDA and gene *sod*. Thus, common photosynthetic goal and oxidative stress explained the synergistic effect of CAP and mPS. Furthermore, molecular dynamics simulation indicated that CAP could insert into the active pocket of photosynthesis-related protein YCF48 and SOD enzyme, which changed the conformation and competed for functional sites of proteins. These findings provide valuable data for combined (antibiotics and MPs) toxicity and mechanism exploration. However, the combined toxicity of antibiotics and MPs is varied, which means it needs to be filled with more research. Additionally, it is insufficient to rely only on physiological biomarkers in toxicity studies. Transcriptomics, proteomics, and metabonomics are beneficial for locating targets of pollutants. Then, the emergence of molecular modeling (molecular docking and molecular dynamics simulation) can further predict interactions between contaminant and target proteins to explore mechanisms at the molecular level.

CRediT authorship contribution statement

Na Li: Conceptualization, Methodology, Formal analysis, Investigation, Visualization, Writing – original draft. **Zhuotong Zeng:** Formal analysis, Data curation, Methodology, Writing – review & editing. **Yafei Zhang:** Formal analysis, Data curation, Methodology, Writing – review & editing. **Hui Zhang:** Writing – review & editing. **Ning Tang:** Writing – review & editing. **Yihui Guo:** Writing – review & editing. **Lan Lu:** Writing – review & editing. **Xin Li:** Writing – review & editing. **Ziqian Zhu:** Writing – review & editing. **Xiang Gao:** Writing – review & editing. **Jie Liang:** Writing – review & editing, Supervision.

Data availability

The authors do not have permission to share data.

Declaration of Competing Interest

The authors declare that they have no known competing financial interests or personal relationships that could have appeared to influence the work reported in this paper.

Acknowledgments

This work was supported by National Natural Science Foundation of China (51979101, 51679082), Hunan Provincial Natural Science Foundation (2019JJ20002) and Resources Department of Hunan Province (XSKJ2021000–06, XSKJ2022068–21).

Appendix A. Supplementary data

Supplementary data to this article can be found online at https://doi.org/10.1016/j.scitotenv.2022.161375.

References

Atzenhofer, W., Regelsberger, G., Jacob, U., Peschek, G.A., Furtmüller, P.G., Huber, R., et al., 2002. The 2.0Å resolution structure of the catalytic portion of a cyanobacterial membrane-bound manganese superoxide dismutase. J. Mol. Bio. 321, 479–489.

Bennett, A., Bogorad, L., 1973. Complementary chromatic adaptation in a filamentous blue-green alga. J. Cell Bio. 58, 419–435.

Bhatt, P., Joshi, T., Bhatt, K., Zhang, W., Huang, Y., Chen, S., 2021. Binding interaction of glyphosate with glyphosate oxidoreductase and C-P lyase: molecular docking and molecular dynamics simulation studies. J. Hazard. Mater. 409, 124927.

Bi, X.D., Zhang, S.L., Zhang, B., Dai, W., Xing, K.Z., 2011. Effects of berberine on the photosynthetic pigments compositions and ultrastructure of cyanobacterium microcystis aeruginosa. Adv. Mater. Res. 343–344, 1117–1125.

Botterell, Z.L.R., Beaumont, N., Cole, M., Hopkins, F.E., Steinke, M., Thompson, R.C., et al., 2020. Bioavailability of microplastics to marine zooplankton: effect of shape and infochemicals. Environ. Sci. Technol. 54, 12024–12033.

Chen, M., Zeng, G., Xu, P., Yan, M., Xiong, W., Zhou, S., 2017. Interaction of carbon nanotubes with microbial enzymes: conformational transitions and potential toxicity. Environ. Sci. Nano 4, 1954–1960.

Feng, L.J., Shi, Y., Li, X.Y., Sun, X.D., Xiao, F., Sun, J.W., et al., 2020. Behavior of tetracycline and polystyrene nanoparticles in estuaries and their joint toxicity on marine microalgae Skeletonema costatum. Environ. Pollut. 263, 114453.

Gopal, C.M., Bhat, K., Ramaswamy, B.R., Kumar, V., Singhal, R.K., Basu, H., et al., 2021. Seasonal occurrence and risk assessment of pharmaceutical and personal care products in bengaluru rivers and lakes, India. J. Environ Chem. Eng. 9.

Hosseini, F.S., Amanlou, M., 2020. Anti-HCV and anti-malaria agent, potential candidates to repurpose for coronavirus infection: virtual screening, molecular docking, and molecular dynamics simulation study. Life Sci. 258, 118205.

Hu, J., Wang, D., Zhang, N., Tang, K., Bai, Y., Tian, Y., et al., 2022. Effects of perfluorooctanoic acid on Microcystis aeruginosa: stress and self-adaptation mechanisms. J. Hazard. Mater. 445, 130396.

Huang, J.N., Wen, B., Xu, L., Ma, H.C., Li, X.X., Gao, J.Z., et al., 2022. Micro/nano-plastics cause neurobehavioral toxicity in discus fish (Symphysodon aequifasciatus): insight from brain-gut-microbiota axis. J. Hazard. Mater. 421, 126830.

Ighodaro, O.M., Akinloye, O.A., 2019. First line defence antioxidants-superoxide dismutase (SOD), catalase (CAT) and glutathione peroxidase (GPX): their fundamental role in the entire antioxidant defence grid. Alexandria J. Med. 54, 287–293.

Jiang, Y., Liu, Y., Zhang, J., 2021. Mechanisms for the stimulatory effects of a five-component mixture of antibiotics in Microcystis aeruginosa at transcriptomic and proteomic levels. J. Hazard. Mater. 406, 124722.

Jin, X., Wu, D., Ling, J., Wang, C., Liu, C., Gu, C., 2019a. Hydrolysis of chloramphenicol catalyzed by clay minerals under nonaqueous conditions. Environ. Sci. Technol. 53, 10645–10653.

Jin, Y., Duan, M., Wang, X., Kong, X., Zhou, W., Sun, H., et al., 2019b. Communication between the ligand-binding pocket and the activation Function-2 domain of androgen receptor revealed by molecular dynamics simulations. J. Chem. Inf. Model. 59, 842–857.

Keren, I.W.Y., Inocencio, J., Mulcahy, L.R., Lewis, K., 2013. Killing by bactericidal antibiotics does not depend on reactive oxygen species. Science 339, 1213–1216.

Kik, K., Bukowska, B., Sicinska, P., 2020. Polystyrene nanoparticles: sources, occurrence in the environment, distribution in tissues, accumulation and toxicity to various organisms. Environ. Pollut. 262, 114297.

Kodru, S., Ur Rehman, A., Vass, I., 2020. Chloramphenicol enhances photosystem II photodamage in intact cells of the cyanobacterium synechocystis PCC 6803. Photosynth. Res. 145, 227–235.

Li, J., Liu, H., Paul, Chen J., 2018a. Microplastics in freshwater systems: a review on occurrence, environmental effects, and methods for microplastics detection. Water Res. 137, 362–374.

Li, S., Shi, W., Liu, W., Li, H., Zhang, W., Hu, J., et al., 2018b. A duodecennial national synthesis of antibiotics in China's major rivers and seas (2005–2016). Sci. Total Environ. 615, 906–917.

Li, S., Wang, P., Zhang, C., Zhou, X., Yin, Z., Hu, T., et al., 2020. Influence of polystyrene microplastics on the growth, photosynthetic efficiency and aggregation of freshwater microalgae Chlamydomonas reinhardtii. Sci. Total Environ. 714, 136767.

Li, G.F., Ma, W.J., Ren, Z.Q., Wang, Y., Li, J.P., Zhao, J.W., et al., 2021. Molecular insight into the binding property and mechanism of sulfamethoxazole to extracellular proteins of anammox sludge. Environ. Sci. Technol. 55, 16627–16635.

Li, X., Luo, J., Zeng, H., Zhu, L., Lu, X., 2022. Microplastics decrease the toxicity of sulfamethoxazole to marine algae (Skeletonema costatum) at the cellular and molecular levels. Sci. Total Environ. 824, 153855.

Lin, W., Yan, Y., Ping, S., Li, P., Li, D., Hu, J., et al., 2021. Metformin-induced epigenetic toxicity in zebrafish: experimental and molecular dynamics simulation studies. Environ. Sci. Technol. 55, 1672–1681.

Liu, H., Zhang, G., Liu, C.Q., Li, L., Xiang, M., 2009. The occurrence of chloramphenicol and tetracyclines in municipal sewage and the Nanming River, Guiyang CityChina. J. Environ. Monit. 11, 1199–1205.

Liu, Y., Chen, S., Zhang, J., Gao, B., 2016. Growth, microcystin-production and proteomic responses of Microcystis aeruginosa under long-term exposure to amoxicillin. Water Res. 93, 141–152.

Liu, Y., Liu, Z., Zeng, G., Chen, M., Jiang, Y., Shao, B., et al., 2018. Effect of surfactants on the interaction of phenol with laccase: molecular docking and molecular dynamics simulation studies. J. Hazard. Mater. 357, 10–18.

Liu, G., Jiang, R., You, J., Muir, D.C.G., Zeng, E.Y., 2020. Microplastic impacts on microalgae growth: effects of size and humic acid. Environ. Sci. Technol. 54, 1782–1789.

Luo, Y., Liang, J., Zeng, G., Li, X., Chen, M., Jiang, L., et al., 2019. Responses of seeds of typical brassica crops to tetracycline stress: sensitivity difference and source analysis. Ecotoxicol. Environ. Saf. 184, 109597.

Mabbitt, P.D., Wilbanks, S.M., Eaton-Rye, J.J., 2014. Structure and function of the hydrophilic photosystem II assembly proteins: Psb27, Psb28 and Ycf48. Plant Physiol. Biochem. 81, 96–107.

Mao, Y., Ai, H., Chen, Y., Zhang, Z., Zeng, P., Kang, L., et al., 2018. Phytoplankton response to polystyrene microplastics: perspective from an entire growth period. Chemosphere 208, 59–68.

Mao, F., He, Y., Gin, K.Y., 2020. Antioxidant responses in cyanobacterium Microcystis aeruginosa caused by two commonly used UV filters, benzophenone-1 and benzophenone-3, at environmentally relevant concentrations. J. Hazard. Mater. 396, 122587.

Okada, K., Satoh, K., Katoh, S., 1991. Chloramphenicol is an inhibitor of photosynthesis. FEBS Lett. 295, 155–158.

Prata, J.C., Lavorante, B., MDC BSMM, Guilhermino L., 2018. Influence of microplastics on the toxicity of the pharmaceuticals procainamide and doxycycline on the marine microalgae tetraselmis chuii. Aquat. Toxicol. 197, 143–152.

Simkin, A.J., Kapoor, L., Doss, C.G.P., Hofmann, T.A., Lawson, T., Ramamoorthy, S., 2022. The role of photosynthesis related pigments in light harvesting, photoprotection and enhancement of photosynthetic yield in planta. Photosynth. Res. 152, 23–42.

Song, Z., Ma, Y.-L., Li, C.-E., Xu, M., 2018. Removal of tetracycline residue from pharmaceutical wastewater by using 3D composite film. Chem. Eng. J. 348, 898–907.

Su, L., Xue, Y., Li, L., Yang, D., Kolandhasamy, P., Li, D., et al., 2016. Microplastics in taihu LakeChina. Environ. Pollut. 216, 711–719.

Trevisan, R., Voy, C., Chen, S., Di Giulio, R.T., 2019. Nanoplastics decrease the toxicity of a complex PAH mixture but impair mitochondrial energy production in developing zebrafish. Environ. Sci. Technol. 53, 8405–8415.

Valitalo, P., Kruglova, A., Mikola, A., Vahala, R., 2017. Toxicological impacts of antibiotics on aquatic micro-organisms: a mini-review. Int. J. Hyg. Environ. Health 220, 558–569.

Wan, J., Guo, P., Peng, X., Wen, K., 2015. Effect of erythromycin exposure on the growth, antioxidant system and photosynthesis of Microcystis flos-aquae. J. Hazard. Mater. 283, 778–786.

Wang, F., Wang, B., Qu, H., Zhao, W., Duan, L., Zhang, Y., et al., 2020a. The influence of nanoplastics on the toxic effects, bioaccumulation, biodegradation and enantioselectivity of ibuprofen in freshwater algae Chlorella pyrenoidosa. Environ. Pollut. 263, 114593.

Wang, X., Hu, M., Gu, H., Zhang, L., Shang, Y., Wang, T., et al., 2020b. Short-term exposure to norfloxacin induces oxidative stress, neurotoxicity and microbiota alteration in juvenile large yellow croaker Pseudosciaena crocea. Environ. Pollut. 267, 115397.

Wang, Y., Yang, Y., Liu, X., Zhao, J., Liu, R., Xing, B., 2021. Interaction of microplastics with antibiotics in aquatic environment: distribution, adsorption, and toxicity. Environ. Sci. Technol. 55, 15579–15595.

Wang, W., Zhang, J., Qiu, Z., Cui, Z., Li, N., Li, X., et al., 2022. Effects of polyethylene microplastics on cell membranes: a combined study of experiments and molecular dynamics simulations. J. Hazard. Mater. 429, 128323.

Wu, Y., Guo, P., Zhang, X., Zhang, Y., Xie, S., Deng, J., 2019. Effect of microplastics exposure on the photosynthesis system of freshwater algae. J. Hazard. Mater. 374, 219–227.

Xiong, Q., Hu, L.X., Liu, Y.S., Wang, T.T., Ying, G.G., 2019. New insight into the toxic effects of chloramphenicol and roxithromycin to algae using FTIR spectroscopy. Aquat. Toxicol. 207, 197–207.

Xiong, Q., Hu, L.X., Liu, Y.S., Zhao, J.L., He, L.Y., Ying, G.G., 2021. Microalgae-based technology for antibiotics removal: from mechanisms to application of innovational hybrid systems. Environ. Int. 155, 106594.

Xu, K., Li, Z., Juneau, P., Xiao, F., Lian, Y., Zhang, W., et al., 2021. Toxic and protective mechanisms of cyanobacterium synechocystis sp. In response to titanium dioxide nanoparticles. Environ. Pollut. 274, 116508.

Yan, C., Yang, Y., Zhou, J., Nie, M., Liu, M., Hochella Jr., M.F., 2015. Selected emerging organic contaminants in the Yangtze estuary, China: a comprehensive treatment of their association with aquatic colloids. J. Hazard. Mater. 283, 14–23.

Ye, T., Yang, A., Wang, Y., Song, N., Wang, P., Xu, H., 2022. Changes of the physicochemical properties of extracellular polymeric substances (EPS) from Microcystis aeruginosa in response to microplastics. Environ. Pollut. 315, 120354.

You, M., You, X., Hu, J., Yang, X., Sun, W., 2021. Carbon nanotubes influence the toxic effects of chloramphenicol and tetracycline on cyanobacterium synechocystis sp. In different ways. Environ. Sci. Nano 8, 634–646.

You, X., Li, H., Pan, B., You, M., Sun, W., 2022. Interactions between antibiotics and heavy metals determine their combined toxicity to synechocystis sp. J. Hazard. Mater. 424, 127707.

Yu, J., Knoppova, J., Michoux, F., Bialek, W., Cota, E., Shukla, M.K., et al., 2018. Ycf48 involved in the biogenesis of the oxygen-evolving photosystem II complex is a seven-bladed beta-propeller protein. Proc. Natl. Acad. Sci. U. S. A. 115, E7824–E7833.

Zeng, H., Hu, X., Ouyang, S., Zhou, Q., 2021. Nanocolloids, but not humic acids, augment the phytotoxicity of single-layer molybdenum disulfide nanosheets. Environ. Sci. Technol. 55, 1122–1133.

Zhang, X., Wang, X., Yan, B., 2021. Single and combined effects of phenanthrene and polystyrene microplastics on oxidative stress of the clam (Mactra veneriformis). Sci. Total Environ. 771, 144728.

Zhang, H., Liang, J., Luo, Y., Tang, N., Li, X., Zhu, Z., et al., 2022a. Comparative effects of polystyrene nanoplastics with different surface charge on seedling establishment of chinese cabbage (Brassica rapa L.). Chemosphere 292, 133403.

Zhang, W., Sun, S., Du, X., Han, Y., Tang, Y., Zhou, W., et al., 2022b. Toxic impacts of microplastics and tetrabromobisphenol a on the motility of marine microalgae and potential mechanisms of action. Gondwana Res. 108, 158–170.

Zhang, X., Liu, N., Lu, H., Zhu, L., 2022c. Molecular mechanism of organic pollutant-induced reduction of carbon fixation and biomass yield in Oryza sativa L. Environ. Sci. Technol. 56, 4162–4172.

Zhang, Y., Li, X., Liang, J., Luo, Y., Tang, N., Ye, S., et al., 2022d. Microcystis aeruginosa's exposure to an antagonism of nanoplastics and MWCNTs: the disorders in cellular and metabolic processes. Chemosphere 288, 132516.

Zheng, X., Liu, X., Zhang, L., Wang, Z., Yuan, Y., Li, J., et al., 2022. Toxicity mechanism of nylon microplastics on Microcystis aeruginosa through three pathways: photosynthesis, oxidative stress and energy metabolism. J. Hazard. Mater. 426, 128094.

Zhou, T., Wang, J., Zheng, H., Wu, X., Wang, Y., Liu, M., et al., 2018. Characterization of additional zinc ions on the growth, biochemical composition and photosynthetic performance from Spirulina platensis. Bioresour. Technol. 269, 285–291.

Zhou, J., Gao, L., Lin, Y., Pan, B., Li, M., 2021a. Micrometer scale polystyrene plastics of varying concentrations and particle sizes inhibit growth and upregulate microcystin-related gene expression in Microcystis aeruginosa. J. Hazard. Mater. 420, 126591.

Zhou, T., Cao, L., Zhang, Q., Liu, Y., Xiang, S., Liu, T., et al., 2021b. Effect of chlortetracycline on the growth and intracellular components of Spirulina platensis and its biodegradation pathway. J. Hazard. Mater. 413, 125310.

Zhu, Z.L., Wang, S.C., Zhao, F.F., Wang, S.G., Liu, F.F., Liu, G.Z., 2019. Joint toxicity of microplastics with triclosan to marine microalgae Skeletonema costatum. Environ. Pollut. 246, 509–517.